atmosphere

MDPI

Article

Sub-Seasonal Prediction of the Maritime Continent Rainfall of Wet-Dry Transitional Seasons in the NCEP Climate Forecast Version 2

Tuantuan Zhang [1], Song Yang [1,2,*], Xingwen Jiang [3] and Shaorou Dong [1]

[1] Department of Atmospheric Sciences, Sun Yat-sen University, Guangzhou 510275, China; zhtuant@mail2.sysu.edu.cn (T.Z.); siyueyuzhiyin@163.com (S.D.)
[2] Institute of Earth Climate and Environment System, Sun Yat-sen University, Guangzhou 510275, China
[3] Institute of Plateau Meteorology, China Meteorological Administration, and Key Laboratory of Heavy Rain and Drought-Flood Disasters in Plateau and Basin of Sichuan Province, Chengdu 610071, China; xingwen.jiang@yahoo.com
* Correspondence: yangsong3@mail.sysu.edu.cn; Tel.: +86-20-8411-1286

Academic Editor: John Boland
Received: 30 November 2015; Accepted: 3 February 2016; Published: 15 February 2016

Abstract: This study investigates the characteristics and prediction of the Maritime Continent (MC) rainfall for the transitional periods between wet and dry seasons. Several observational data sets and the output from the 45-day hindcast by the U.S. National Centers for Environmental Prediction (NCEP) Climate Forecast System version 2 (CFSv2) are used. Results show that the MC experiences a sudden transition from wet season to dry season (WTD) around the 27th pentad, and a gradual transition from dry season to wet season (DTW) around the 59th pentad. Correspondingly, the westerlies over the equatorial Indian Ocean, the easterlies over the equatorial Pacific Ocean, and the Australia High become weaker, contributing to weakening of the convergence over the MC. The subtropical western Pacific high intensifies and extends northeastward during the WTD. The Mascarene High becomes weaker, an anomalous anticyclonic circulation forms over the northeast of the Philippines, and an anomalous low-level convergence occurs over the western MC during the DTW. The NCEP CFSv2 captures the major features of rainfall and related atmospheric circulation when forecast lead time is less than three weeks for WTD and two weeks for DTW. The model predicts a weaker amplitude of the changes in rainfall and related atmospheric circulation for both WTD and DTW as lead time increases.

Keywords: the maritime continent; transitional periods; rainfall prediction

1. Introduction

The Maritime Continent (MC) is a "land bridge" connecting the continental areas of East/Southeast Asia and Australia, and it consists of multiple islands of Southeast Asia including Sumatra, Java, Borneo, and New Guinea and oceanic areas of the equatorial western Pacific [1–7]. The MC is located in the core of the strongest monsoon region of the world, and lies within the area of the warmest ocean which leads to large amounts of moist convection and heat release that favor rising motion over the region [7–16]. Thus, the MC plays an important role in variations of global climate [13–31]. For example, latent heat release from rainfall or convective activity over the MC modulates the rainfall over East Asia through the Hadley cell, and favors tropical cyclone formation [2,23,24,26].

The annual cycle of rainfall over the MC features distinct dry and wet seasons, with asymmetric seasonal transitions [1,32–38]. Maximum convection gradually moves southeastward from the north of

the MC to southern MC and northern Australia along the "land bridge" during the boreal fall, while it does not return to the north of the MC in the same way during the boreal spring [1]. The transition from wet season to dry season is very quick but the reverse process is relatively gradual. Chang *et al.* [1] proposed that this asymmetry was due to the mass distributions between the two transitional seasons and an asymmetric low-level divergence over the region. Matsumoto and Murakami [5,38] indicated that the cold surges during the boreal spring (originating from Australia) were weaker than those during the boreal fall (originating from East Asia), and the respective annual variations of the equatorial basic flows over the Indian Ocean and western Pacific contributed to this asymmetry.

The latent heat released from the rainfall over the MC is important for the maintenance of the Walker circulation and local Hadley circulation. Thus, the change in rainfall between the dry and wet seasons results in changes in local and remote rainfall and circulation. The onset of the Asian summer monsoon is characterized by an abrupt northward jump of the rainfall band over the equatorial MC [39]. Thus, understandings of the transition between dry and wet seasons over the MC provide insights into the onset of the Asian summer monsoon, among others. Besides, the timing of the transition between dry and wet is important for agricultural activity because of the large difference in rainfall between the dry and wet seasons. However, the transition between dry and wet seasons has received less attention compared to the diurnal cycle of rainfall, the interannual variation of rainfall in wet and dry seasons, and the interactions of MC rainfall with the Madden-Jullian Oscillation (MJO; intraseasonal) and El Niño-Southern Oscillation (ENSO; interannual). As a result, many features of the transition of MC rainfall between dry and wet seasons remain unclear.

Dynamical models now are very useful tools for weather and climate forecasts. However, realistic prediction of the MC rainfall is still a big challenge for dynamical models. Previous studies have revealed a robust dry bias over the MC for wet and dry seasons and indicated that the dry bias exists in most dynamical models [40–45]. Spatially incoherent rainfall over the MC in the wet season leads to an "incoherent unpredictable" feature, especially for the western MC rainfall which tends to be uncorrelated with the sea surface temperature (SST) in the wet season [29,31]. Moreover, several studies have reported that a deficient representation of rainfall (or convection) exists in dynamical models [46–48]. Besides, most models have difficulties in predicting the propagation of MJO through the MC into the Pacific Ocean, which is referred to as the MJO "Maritime Continent prediction barrier" problem [17,49–52]. Nevertheless, most focus has been placed on the prediction of rainfall (or convection) in wet and dry seasons over the MC, but how well the transition between the two seasons can be predicted by dynamical models is unknown by far.

As a fully coupled forecast system and one of the state-of-the-art operational climate models, the United States National Centers for Environmental Prediction (NCEP) Climate Forecast System version 2 (CFSv2) has provided an important source of information for global and regional climate prediction [53–55]. It has exhibited considerable skill in the monthly and seasonal prediction of climate over the Asian-Pacific regions including the MC. Moreover, the CFSv2 hindcasts consist of not only monthly mean data but also daily data and thus provide a good opportunity for investigating the predictability and the skill of prediction of sub-seasonal climate phenomena such as the transition between dry and wet seasons for the MC.

In this study, we first analyze the variation of rainfall during the transition seasons and associated large-scale circulation, and then investigate their predictions by the CFSv2. The rest of this paper is organized as follows. The introduction of the model and data sets applied in this study is given in Section 2. Section 3 provides an assessment of the major features of the MC rainfall of the transitional periods between wet and dry seasons and the prediction of these features by the CFSv2 of zero-day lead. The skills of prediction of these transitional features in different leads of time are discussed in Section 4. Finally, a summary of the results obtained and a further discussion are provided in Section 5.

2. Model and Data

The NCEP CFSv2 is a fully coupled dynamical prediction system and one of the state-of-the-art operational climate models [53–55]. It consists of the NCEP Atmospheric Global Forecast System with 64 sigma layers in the vertical and a T126 resolution in the horizontal as its atmospheric component [56]; the NCEP, Oregon State University (OSU), the Air Force, and the Hydrologic Research Laboratory land model Noah [57]; and the Modular Ocean Model version 4.0 from the Geophysical Fluid Dynamics Laboratory of the National Oceanic and Atmospheric Administration as its oceanic component [58]. We analyze the output of rainfall and 850-hPa winds from the retrospective forecasts of 45-day integrations from the CFSv2 (initiated from every 0000 Coordinated Universal Time (UTC), 0600 UTC, 1200 UTC, and 1800 UTC cycle) from 2000 to 2010. For a specific predicted target day, the longest lead time is 44 days. The zero-day lead denotes that the model runs initialized on this day while the 44-day lead denotes that the model runs initialized 44 days ago. We calculate pentad mean from the daily data because the daily mean is too noisy to determine the transitional date while the pentad mean can be considered a simple filter to remove the weather signals and is thus widely used to analyze seasonal transition [39]. There are 73 pentads for each year (February 29 is not included for leap years) [59]. The first pentad is for 1–5 January, and the last pentad is for 27–31 December. As an example, for the 73rd pentad zero-day lead, the ensemble mean of the runs initialized from 27, 28, 29, 30, and 31 December is used as the forecast. For the 73rd pentad 44-day lead (the longest lead time), the ensemble mean of the runs initialized from 13, 14, 15, 16, and 17 November is used as the forecast. For convenience, the zero-day lead, one-day lead, two-day lead, . . . , and 44-day lead of the CFSv2 are denoted as LD0, LD1, LD2, . . . , and LD44, respectively.

The observations used for model verification include daily precipitation from the Global Precipitation Climatology Project (GPCP) with a horizontal resolution of 1° [60], and winds and 500-hPa geopotential height with 0.5° horizontal resolution from the Climate Forecast System Reanalysis (CFSR) [55]. In this study, the MC region is defined as the domain of (9°S–1°S/98°E–145°E plus 1°S–7°N/98°E–120°E).

3. Prediction of MC Rainfall of the Transitional Periods between Wet and Dry Seasons in LD0

3.1. Major Features in Observation

Figure 1a shows the climatological (2000–2010) pentad-mean rainfall over the MC, in which the black solid line denotes observed values. MC rainfall exhibits strong seasonal variations, with distinct dry and wet seasons. The annual mean of observation is about 6.5 mm/day, while the minimum value of the pentad mean rainfall is below 4 mm/day in the 44th pentad and the maximum rainfall is above 10 mm/day in the 73rd pentad. The transition between dry and wet seasons is asymmetric. A sudden decrease (about 4.5 mm/day) happens from the 26th pentad to the 28th pentad, while an increase with smaller amplitude (about 2 mm/day) occurs from the 58th pentad to the 60th pentad. It is not easy to define the transition date between dry and wet seasons objectively because the MC rainfall exhibits remarkable intraseasonal variations. To better reflect the overall difference in rainfall between dry and wet seasons and exclude the effect of the intraseasonal oscillation, we define the transition date between the wet season to dry season (dry season to wet season) as the pentad that satisfies the following criteria: (1) the first pentad when rainfall is below (above) the annual mean during the 17th–37th (49th–69th) pentad; (2) rainfall in the consecutive three pentads following the first pentad is below the annual mean; and (3) averaged rainfall for the first pentad and following five pentads is below (above) the annual mean. For convenience, the transition from wet season to dry season (from dry season to wet season) is briefly denoted as WTD (DTW). Thus, the WTD occurs around the 27th pentad and the DTW occurs around the 59th pentad according to the above definition. We also calculated climatological pentad-mean rainfall for 36 years (1979–2014) using the pentad data from the Climate Prediction Center Merged Analysis of Rainfall (CMAP) and GPCP and found the annual cycle of rainfall over the MC depicted by the two data sets is similar to that shown in Figure 1,

demonstrating that the results revealed by the above analysis are reliable (figure not shown). It should also be noticed that the northeastern MC is not included in this study due to the different features of rainfall variation (figure not shown) over this region compared to other regions of the MC, and part of the northeastern MC is included in the Asian-Pacific summer monsoon regime [61].

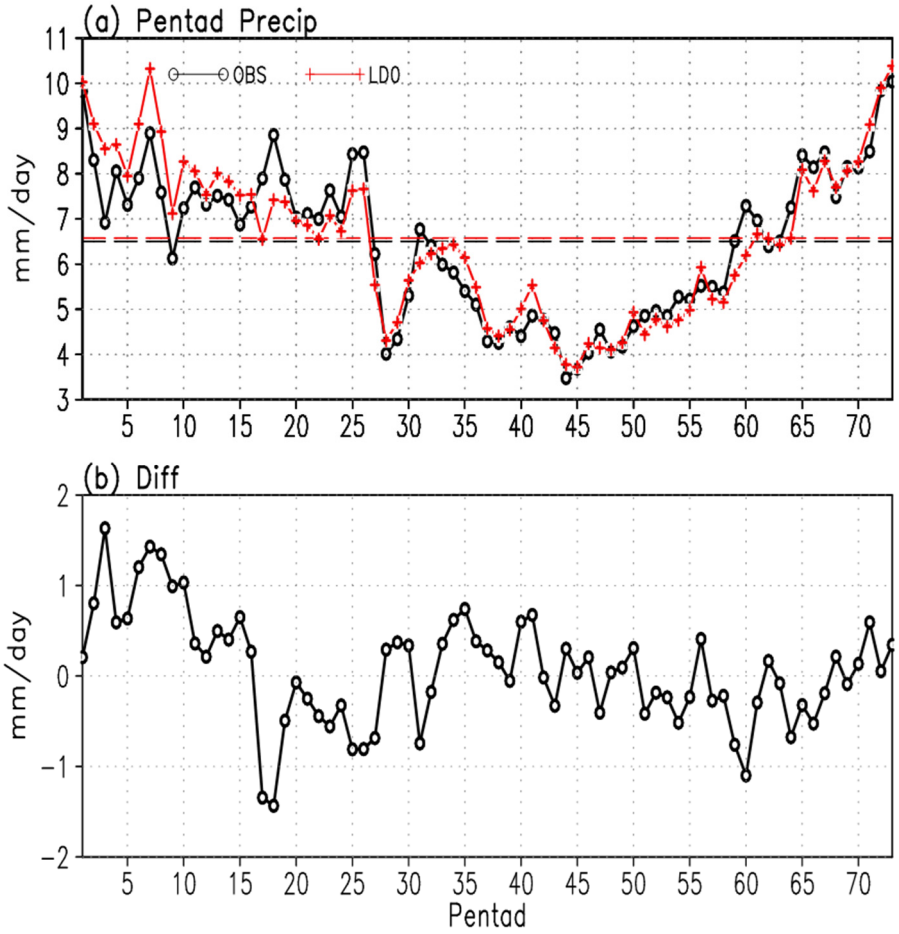

Figure 1. (**a**) Climatological pentad mean rainfall (mm/day) averaged over the Maritime Continent (9°S–1°S/98°E–145°E plus 1°S–7°N/98°E–120°E) for observation (GPCP; black line) and CFSv2 LD0 (red line); (**b**) Difference of climatological pentad mean rainfall (mm/day) between CFSv2 LD0 and observation (GPCP). The horizontal black line and red line denote the annual mean values for observation and the CFSv2, respectively.

Figure 2a shows the time-latitude cross-sections of climatological pentad-mean rainfall and 850-hPa winds along the longitudes of MC in observations. The rainfall amount is above 7 mm/day over the MC, except in the north of 2.5°N during the first pentad to the 26th pentad, and then experiences a sudden decrease around the 27th pentad. Rainfall over the MC is almost below 7 mm/day from the 27th pentad to the 58th pentad, with the driest region over the south of 5°S. Rainfall gradually increases from the northern MC to southern MC from the 58th pentad to the 73rd pentad. Correspondingly, northeasterly and northwesterly low-level winds are seen over the north and south of 2.5°N from the first pentad to the 26th pentad, and southwesterly and southeasterly winds appear from the 27th pentad to the 58th pentad. Winds gradually turn to northerly or westerly flows from the northern MC to the southern MC after the 59th pentad.

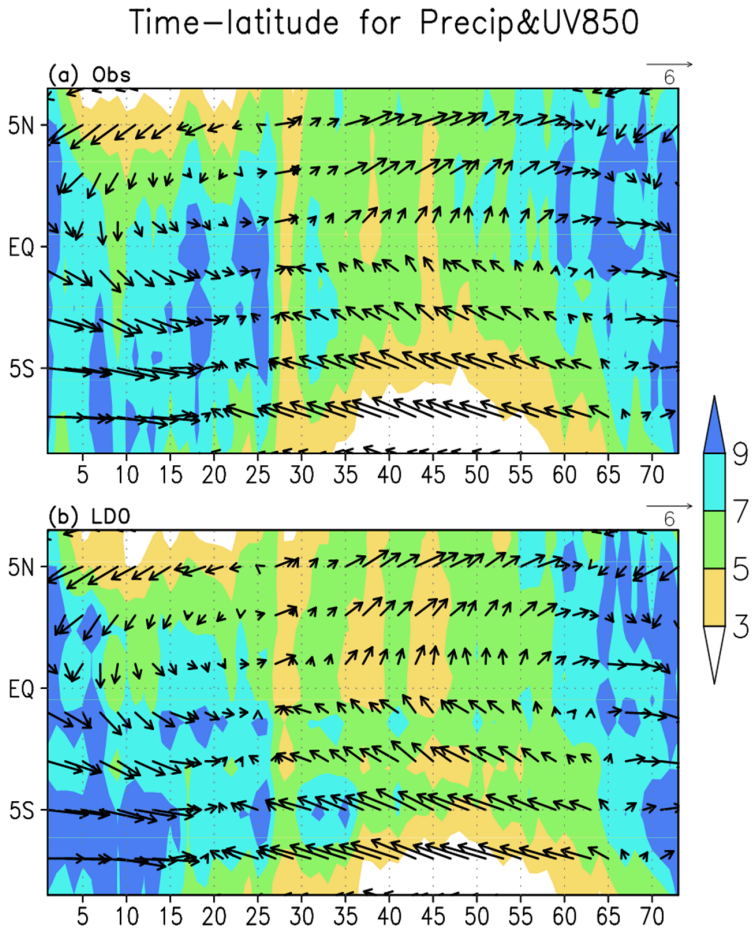

Figure 2. Time-latitude cross-sections of climatological pentad mean rainfall (GPCP; shadings; mm/day) and 850-hPa winds (CFSR; vectors; m/s) along the longitudes (98°E–145°E for 9°S–1°S and 98°E–120°E for 1°S–7°N) of Maritime Continent from the first pentad to the 73rd pentad (x-coordinate) for (**a**) observations; and (**b**) CFSv2 LD0 prediction.

A question from the above analysis is what happens during the WTD and the DTW. The pentad means of rainfall and 850-hPa winds from the 25th pentad to the 29th pentad and the differences between the 28th–29th pentad mean and the 25th–29th pentad mean are shown in Figure 3. It can be seen from Figure 3a,b that the westerlies over the equatorial Indian Ocean, the easterlies over the equatorial Pacific Ocean, and the southeasterly winds from the Australia High converge in over the MC, accompanied by heavy rainfall over the MC during the 25th–26th pentads when heavy rainfall is mainly centered over islands. The rain belt jumps northward to the South China Sea from the 26th pentad to the 27th pentad, associated with the enhancement of southwesterly winds from the Arabian Sea to the South China Sea (Figure 3c). The rainfall over the MC decreases from the 27th pentad to the 29th pentad (Figure 3c–e). More specifically, rainfall decreases over the low latitudes between 60°E to 160°E and increases over the north of the MC during the WTD, accompanied by an enhancement of the southeasterly monsoon winds and a weakening of the easterly winds and westerly winds over the equatorial Indian Ocean and the equatorial Pacific Ocean. The Australia High weakens as well. These changes in atmospheric circulation contribute to anomalous divergence (or weakening of convergence) over the MC during the WTD (Figure 3f). Examinations of the 500-hPa geopotential height and 200-hPa winds from the 25th pentad to the 29th pentad also indicate that the western Pacific subtropical high (WPSH) intensifies and extends northward and eastward and an anomalous convergence forms over the MC during the WTD (Figure 4).

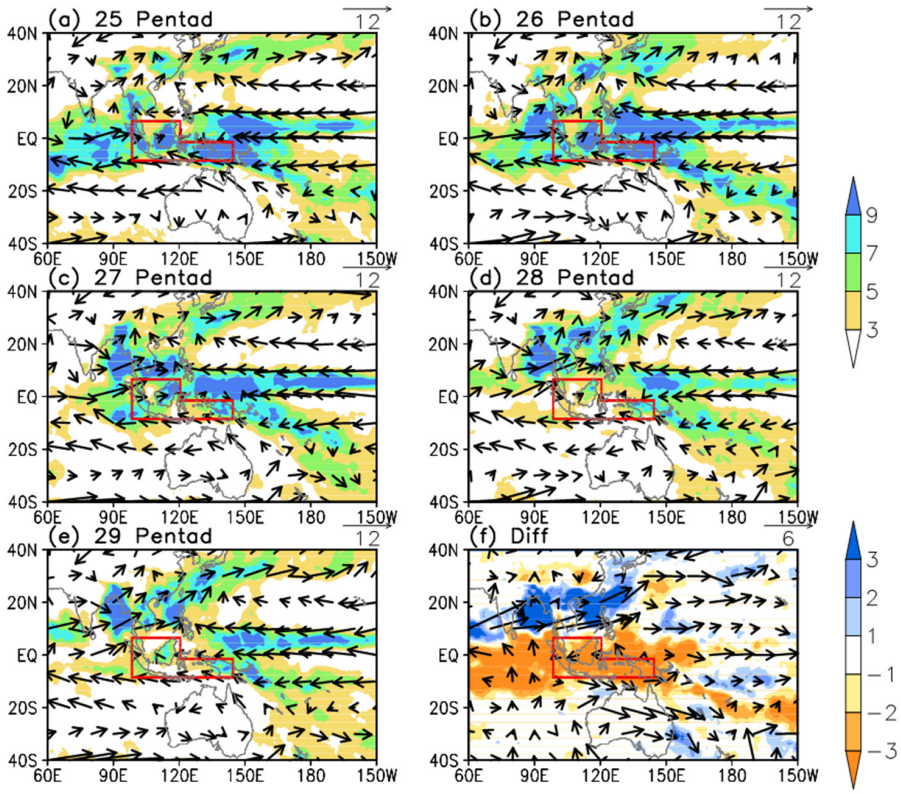

Figure 3. Climatological mean rainfall (GPCP; shading; mm/day) and 850-hPa winds (CFSR; vectors; m/s) for (**a**) 25th pentad; (**b**) 26th pentad; (**c**) 27th pentad; (**d**) 28th pentad; and (**e**) 29th pentad; (**f**) Differences between 28th–29th pentad mean and 25th–26th pentad mean. The domain of the Maritime Continent is outlined with red boxes.

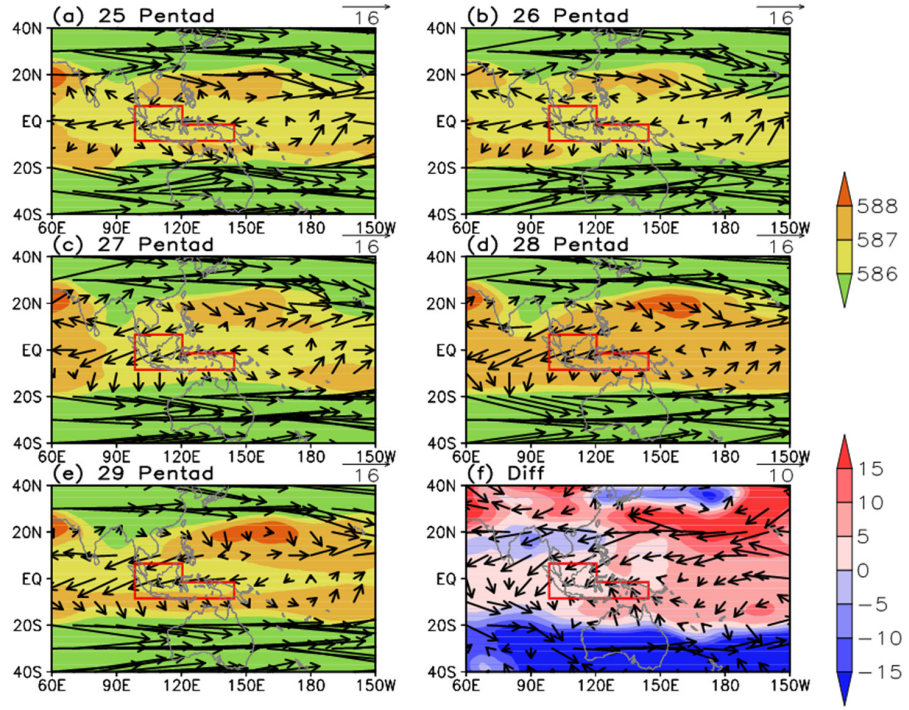

Figure 4. Same as in Figure 3, but for 500-hPa geopotential height (CFSR; dgpm; shading) and 200-hPa winds (CFSR; m/s; vectors).

Figure 5 shows pentad mean and difference patterns for the DTW. During the 57th pentad and the 58th pentad, westerlies over the northern Indian Ocean and easterlies from the western Pacific Ocean to the Indo-China Peninsula converge around the South China Sea, and a weak cyclonic circulation forms over the Bay of Bengal (Figure 5a,b). Correspondingly, the rain band is mainly located over the north of the equator (Figure 5a,b). Rainfall increases over the western MC and the cyclonic circulation over the Bay of Bengal disappears in the 59th pentad (Figure 5c). Heavy rainfall moves southward gradually, and easterly winds over the western Pacific Ocean extend westward from the 59th pentad to the 61st pentad (Figure 5c–f). It can be found from the difference patterns that the Mascarene High weakens during the DTW and an anomalous anticyclonic circulation appears to the northeast of the Philippines. As a result, an anomalous divergence forms over the northeast of the Philippines and an anomalous convergence appears over the northern Indian Ocean (Figure 5f). Correspondingly, a negative rainfall difference appears over the north of the MC and a positive rainfall difference emerges from the northern Indian Ocean (Figure 5f). However, the difference patterns for the DTW are not completely opposite to those for the WTD, and a negative rainfall difference even appears over the southeastern MC (Figure 5f). This spatial incoherent variation of rainfall during the DTW is due to the gradual increase in rainfall from the northern MC to the southern MC (see Figure 2), and from the western MC to the eastern MC, contributing to a later transition from dry season to wet season over the southeastern MC (figures not shown). Besides, the upper-level patterns for the DTW show that the WPSH weakens and the difference in 200-hPa winds converge around the MC region, and an anomalous high forms over the northeast of the Philippines during the DTW (Figure 6).

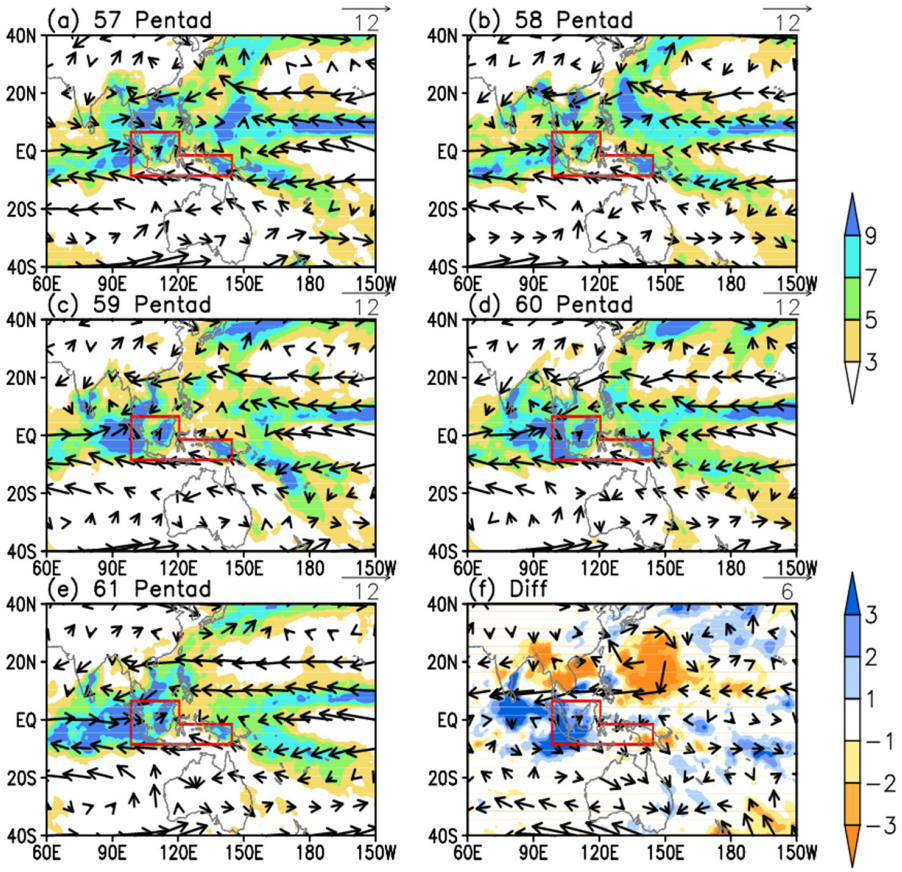

Figure 5. Climatological mean rainfall (GPCP; shading; mm/day) and 850-hPa winds (CFSR; vectors; m/s) for (**a**) 57th pentad; (**b**) 58th pentad; (**c**) 59th pentad; (**d**) 60th pentad; and (**e**) 61st pentad; (**f**) Differences between 60th–61st pentad mean and 57th-58th pentad. The domain of the Maritime Continent is outlined with red boxes.

3.2. Prediction in LD0

Due to the unique location, complex distribution of land, sea, and topography, as well as the important role of the MC in atmospheric circulation, previous efforts have also been devoted to understanding the prediction of the MC climate [29,31,37,40,45]. However, few studies have been conducted on the predictions of the MC rainfall and associated circulation patterns during transitional periods.

The red solid line and the horizontal red dashed line in Figure 1a denote the climatological pentad-mean and yearly-mean MC rainfall for CFSv2 LD0, respectively. The sub-seasonal variations of rainfall in LD0 are generally similar to those observed, particularly during the dry season and from the 65th pentad to the 73rd pentad (Figure 1a). The transition from wet season to dry season around the 27th pentad is well captured by the model, although the magnitude of rainfall decrease is weaker than that in observation. However, the DTW in LD0 is later and weaker than that in the observation (Figure 1a). The annual mean of MC rainfall in LD0 is slightly overestimated compared to the observation, due mainly to the overestimation of MC rainfall from the first pentad to the 16th pentad (Figure 1b). The amount of the MC rainfall is well predicted by the CFSv2 in LD0 from the 19th pentad to 73rd pentad (Figure 1b).

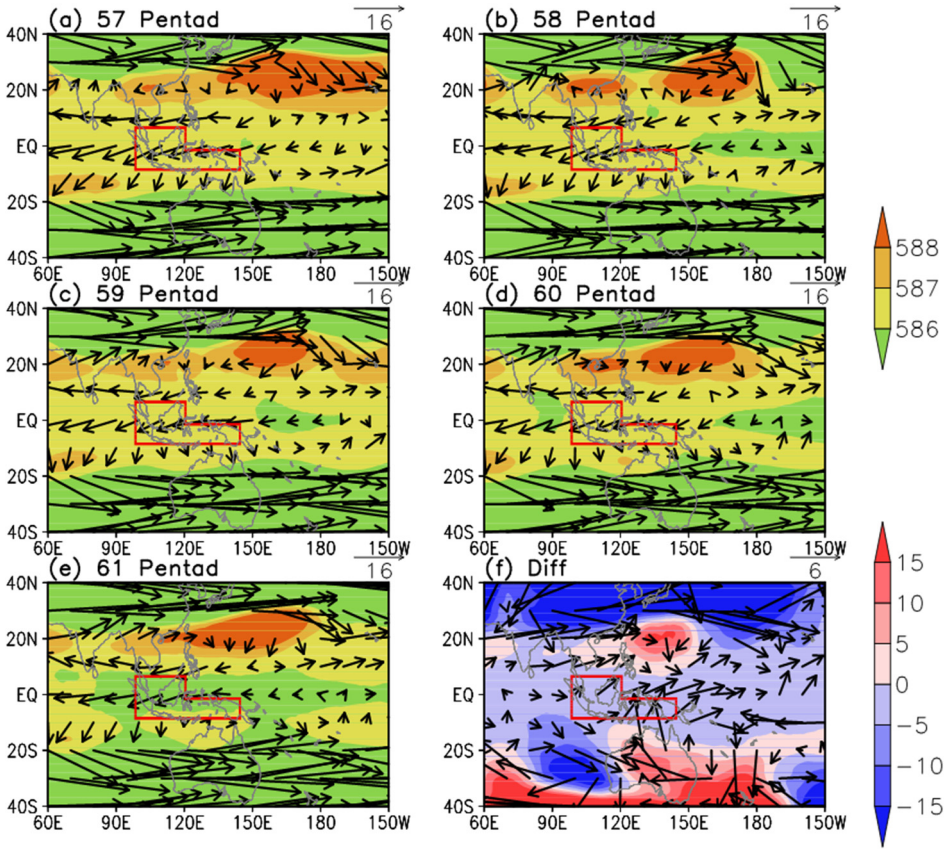

Figure 6. Climatological-mean 500-hPa geopotential height (CFSR; dgpm; shading) and 200-hPa winds (CFSR; m/s; vectors) for (**a**) 57th pentad; (**b**) 58th pentad; (**c**) 59th pentad; (**d**) 60th pentad; and (**e**) 61st pentad; (**f**) Differences between 60th–61st pentad mean and 57th–58th pentad mean. The domain of the Maritime Continent is outlined with red boxes.

Figure 2b shows the time-latitude cross-sections of climatological pentad-mean rainfall and 850-hPa winds in CFSv2 LD0. The model generally predicts the periods of wet season and dry season, particularly for the dry season and from the 65th pentad to the 73rd pentad, consistent with the result

of Figure 1a. However, the CFSv2 overestimates the rainfall to the south of the equator from the first pentad to the 16th pentad (consistent with the result of Figure 1a), and underestimates the rainfall to the south of 2.5°N from the 17th pentad to the 26th pentad, contributing to a smaller decrease in rainfall during the WTD. Besides, less-than-observed rainfall appears to the north of the equator from the 54th pentad to the 60th pentad, which contributes to a later DTW and a smaller increase in rainfall for DTW (Figure 2b). In addition, the model generally captures the major features of low-level atmospheric circulation, including the northeasterly and northwesterly winds during the wet season, and the southeasterly and southwesterly winds during the dry season. It should be noticed that the southwesterly winds to the south of the equator from the first pentad to the 16th pentad are overestimated, consistent with the overestimation of rainfall (Figure 2b).

Climatological pentad mean and difference patterns of rainfall and 850-hPa winds for the WTD in LD0 are shown in Figure 7. Compared with the patterns in observations (Figure 3), the model captures the major features of the WTD such as the locations of the rain belt, the westerlies over the Indian Ocean, the easterlies over the western Pacific Ocean, the development of southwesterly monsoon flow, and the Australia High from the 25th pentad to the 29th pentad (Figures 3 and 7). Also, the changes in the MC rainfall and the associated circulation patterns are similar to those in the observations (Figure 7f). However, less-than-observed rainfall appears over the MC, especially for the islands, during the 25th pentad and the 26th pentad (Figure 7a,b), and more-than-observed rainfall appears over New Guinea from the 27th pentad to the 29th pentad (Figure 7c–e). The CFSv2 overestimates the Intertropical Convergence Zone (ITCZ) rainfall from the 25th pentad to the 29th pentad, as well as the rainfall over the northern Indian Ocean during the 25th pentad and the 26th pentad (Figure 7a–e). Besides, the model captures the upper-level patterns for WTD (figure not shown) well, including intensification of the WPSH and the divergence of the 200-hPa winds over the MC. However, the WPSH is weaker in CFSv2 than in the observation, consistent with the result of Jiang *et al.* [41].

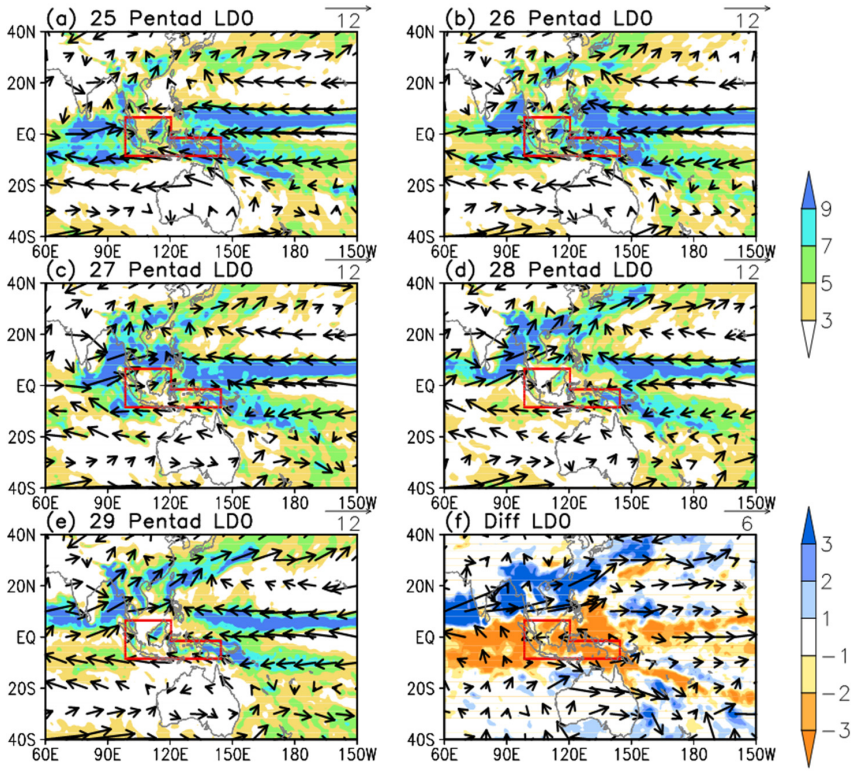

Figure 7. Same as in Figure 3, but for CFSv2 LD0. (**a**) 25th pentad; (**b**) 26th pentad; (**c**) 27th pentad; (**d**) 28th pentad; and (**e**) 29th pentad; (**f**) Differences between 28th–29th pentad mean and 25th–26th pentad mean.

It can be seen from Figure 8, which presents the climatological pentad mean and difference patterns of rainfall and 850-hPa winds for the DTW in LD0, that the locations of the rain belt and associated atmospheric circulation are reasonably captured by the CFSv2 (Figure 8). However, the model underestimates the MC rainfall during the 60th pentad and the 61st pentad (Figure 8d,e), and heavy rainfall occurs over the southern Bay of Bengal in LD0 while it is located near the southwestern MC (in the 60th pentad) in the observation (Figure 8d). The model also overestimates the rainfall over the western Pacific, including the ITCZ and the Southern Pacific Convergence Zone (SPCZ) rainfall (Figure 8a–e). As seen from the difference patterns, the model underestimates the increase in rainfall during the DTW (Figure 8f). The 500-hPa geopotential height and 200-hPa wind patterns are well captured by the model, although the WPSH and the 200-hPa convergence in wind differences are weaker than observed (figure not shown).

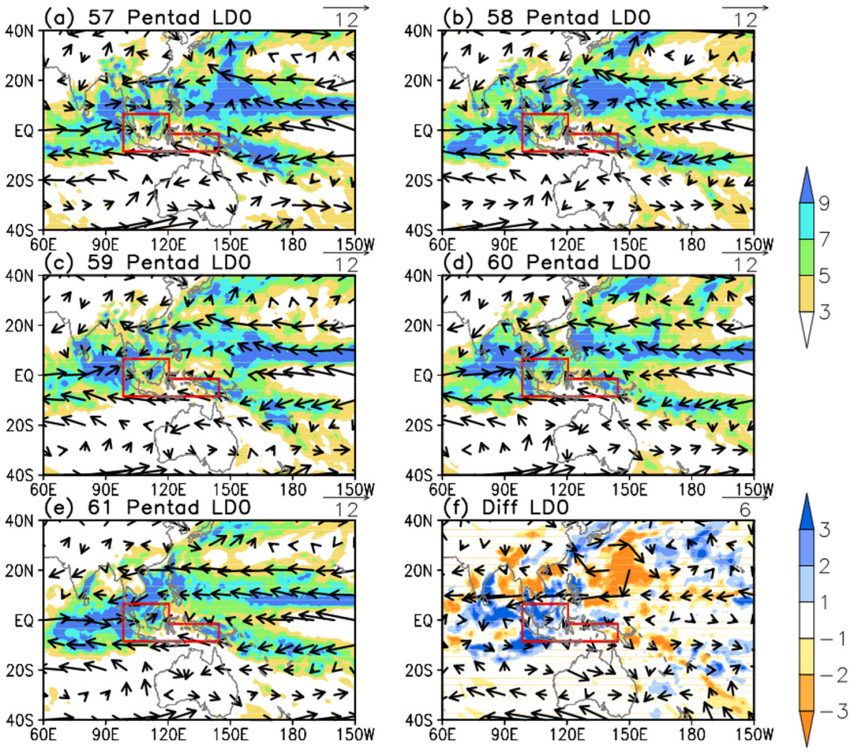

Figure 8. Same as in Figure 5, but for CFSv2 LD0. (**a**) 57th pentad; (**b**) 58th pentad; (**c**) 59th pentad; (**d**) 60th pentad; and (**e**) 61st pentad; (**f**) Differences between 60th–61st pentad mean and 57th–58th pentad mean. The domain of the Maritime Continent is outlined with red boxes.

4. Prediction of MC Rainfall and Associated Circulation Patterns in Different Leads of Time

Figure 9 presents the climatological pentad-mean rainfall averaged over the MC for observation (black solid line) and CFSv2 predictions of different leads of time (red solid line). An overestimation of the MC annual mean rainfall can be seen before LD15, and an underestimation appears when the lead time is longer than 15 days. The model predicts more-than-observed rainfall for almost all pentads when the lead time is shorter than 10 days. After that, the MC rainfall is underestimated from the 15th pentad to the 26th pentad and from the 50th pentad to the 73th pentad. The model overestimates the MC rainfall again from the 27th pentad to the 40th pentad. Correspondingly, the amplitudes of rainfall decrease during WTD and rainfall increase during DTW become smaller as the lead time increases. The model generally captures the major feature of rainfall variation for WTD within 20 lead days (about three weeks), and predicts the feature of rainfall variation for DTW within 15 lead days (about two weeks) well.

Variations of rainfall are always accompanied by changes in atmospheric circulation (Figures 3–6). To investigate how well the variations of related atmospheric circulation can be predicted by the model, time series of climatological pentad mean $\nabla \cdot$ Vh averaged over the MC for both observation and CFSv2 of different leads are shown (Figure 10). Convergence over the MC is much weaker during the WTD and gradually becomes stronger during the DTW in observation (black line in Figure 10), corresponding to the variations of the MC rainfall during WTD and DTW. Change in $\nabla \cdot$ Vh for the DTW is much smaller and slower than that for the WTD. These features are well predicted by the model in a short time lead. However, the model unrealistically predicts the changes in convergence over the MC during WTD (DTW) when the lead time is longer than 20 days (15 days), consistent with the prediction of the MC rainfall variation during the WTD and the DTW.

The changes in rainfall and 850-hPa winds during the WTD for CFSv2 predictions in different leads of time are shown in Figure 11. The difference patterns are similar to those in observations when the lead time is within 10 days. A negative difference center of rainfall is mainly located to the west of the MC when the lead time is longer than 10 days and the negative difference of rainfall over the MC is underestimated by the model. When the lead time is longer than 25 days, a positive difference of rainfall appears over the southeastern MC and then expands to the entire MC due to the southward expansion of the positive rainfall difference over the western Pacific Ocean. The positive difference of rainfall over the Arabian Sea is overestimated by the CFSv2 for all leads. Correspondingly, the southwesterly monsoon winds expand more southward and the difference is smaller from the Bay of Bengal to the western Pacific Ocean in the model than that in the observations. The difference patterns of low-level winds over the western Pacific Ocean are almost opposite to those in the observations, and they are westerly winds in the observations but easterly winds in the model, when lead time is longer than 25 days (Figure 11). The winds over the equatorial Indian Ocean are well captured by the model for all leads.

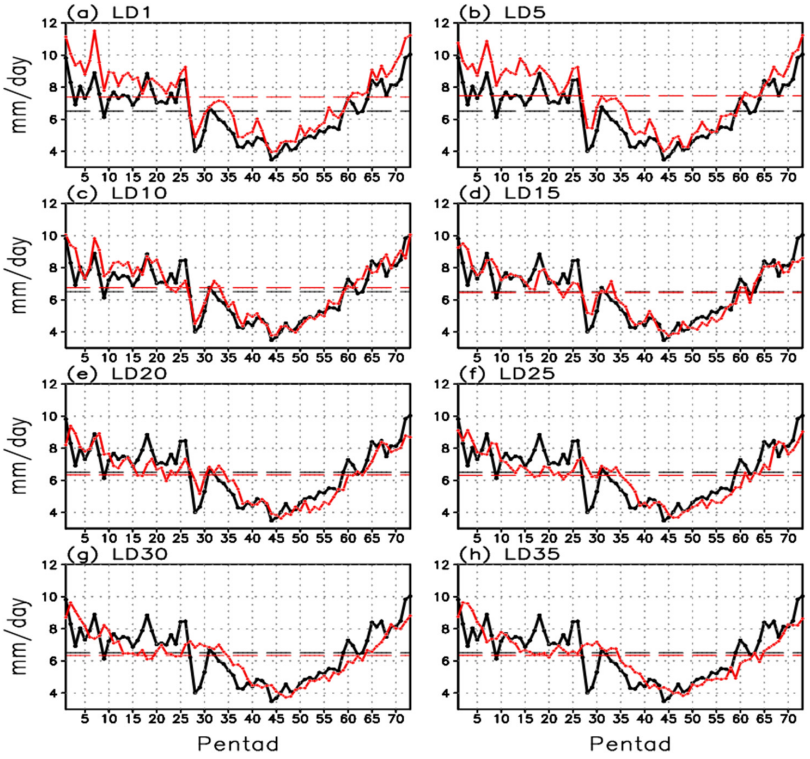

Figure 9. Climatological pentad mean rainfall (mm/day) averaged over the Maritime Continent for observation (GPCP; black line) and CFSv2 predictions (red line) in (**a**) LD1; (**b**) LD5; (**c**) LD10; (**d**) LD15; (**e**) LD20; (**f**) LD25; (**g**) LD30; and (**h**) LD35.

The changes in rainfall and 850-hPa winds during the WTD for CFSv2 predictions in different leads of time are shown in Figure 11. The difference patterns are similar to those in observations when the lead time is within 10 days. A negative difference center of rainfall is mainly located to the west of the MC when the lead time is longer than 10 days and the negative difference of rainfall over the MC is underestimated by the model. When the lead time is longer than 25 days, a positive difference of rainfall appears over the southeastern MC and then expands to the entire MC due to the southward expansion of the positive rainfall difference over the western Pacific Ocean. The positive difference of rainfall over the Arabian Sea is overestimated by the CFSv2 for all leads. Correspondingly, the southwesterly monsoon winds expand more southward and the difference is smaller from the Bay of Bengal to the western Pacific Ocean in the model than that in the observations. The difference patterns of low-level winds over the western Pacific Ocean are almost opposite to those in the observations, and they are westerly winds in the observations but easterly winds in the model, when the lead time is longer than 25 days (Figure 11). The winds over the equatorial Indian Ocean are well captured by the model for all leads.

Differences in rainfall and 850-hPa winds between the 60th–61st pentad mean and the 57th–58th pentad mean (DTW) for CFSv2 predictions in different leads are shown in Figure 12. The model captures the major features of the difference patterns for the DTW within 15-day leads, including the increase in rainfall from the western Indian Ocean to the western MC, and the decrease in rainfall from the Bay of Bengal to the western Pacific Ocean. The model predicts a much weaker decrease and increase of rainfall when the lead time is longer than 15 days. The model also underestimates the anomalous anticyclonic circulation over the western Pacific Ocean and the change in the Mascarene High, contributing to the underestimation of rainfall change over the MC during the DTW.

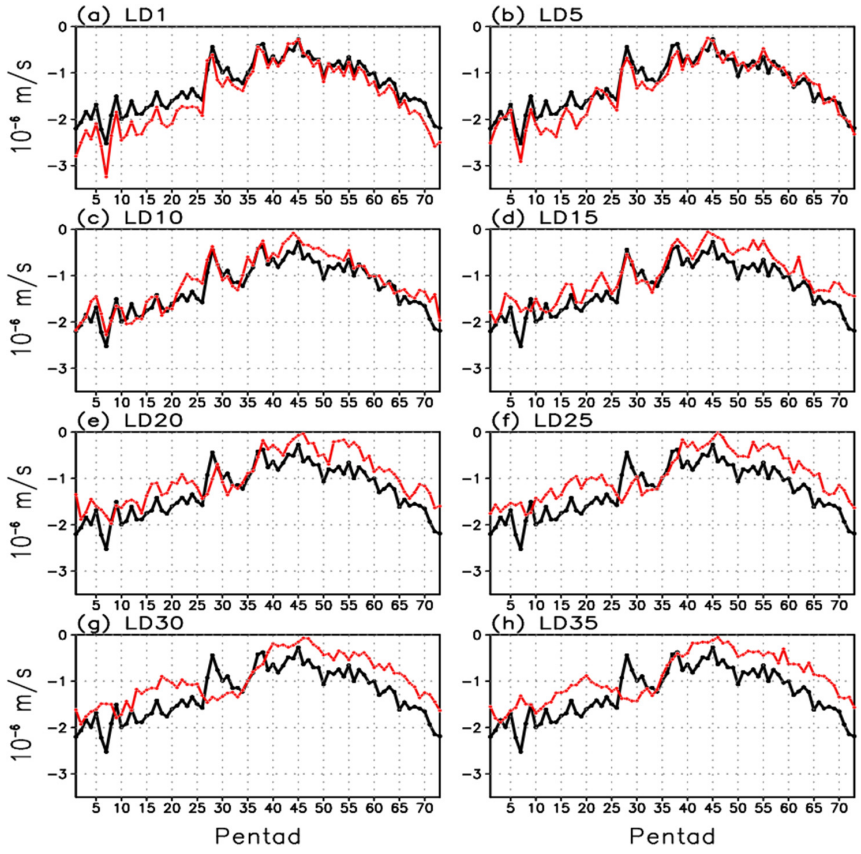

Figure 10. Same as in Figure 9, but for $\nabla \cdot$ Vh (10−6/s)). (**a**) LD1; (**b**) LD5; (**c**) LD10; (**d**) LD15; (**e**) LD20; (**f**) LD25; (**g**) LD30; and (**h**) LD35.

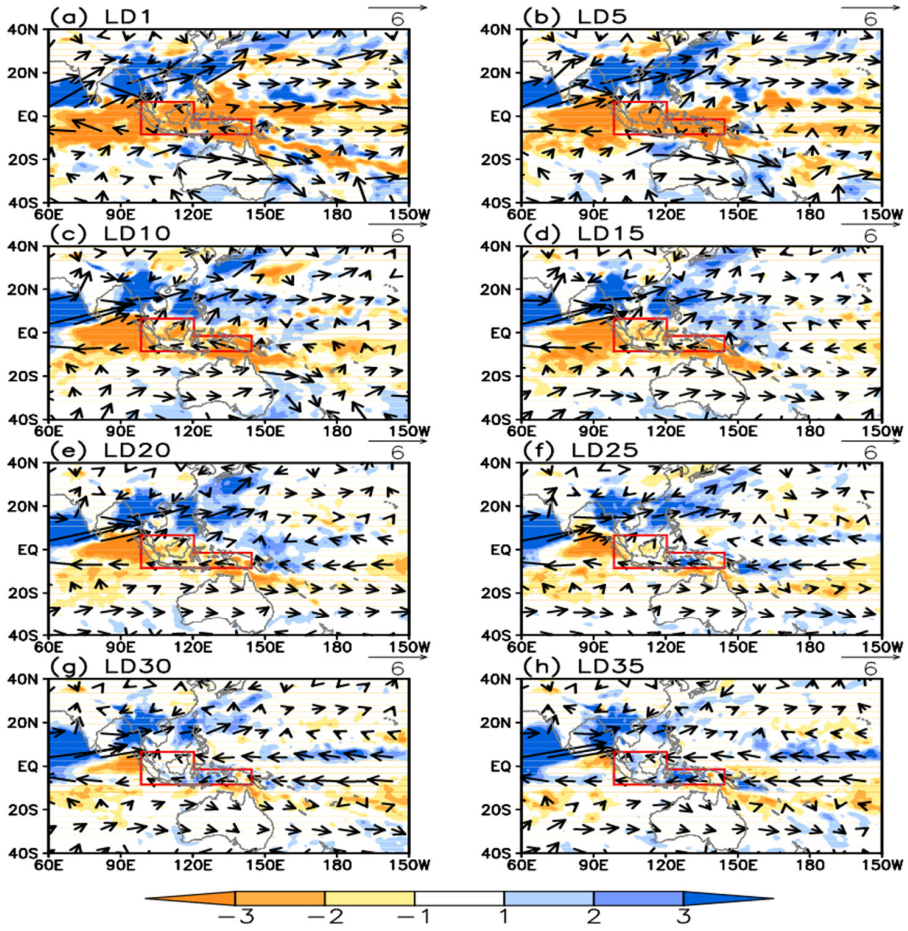

Figure 11. Differences in rainfall (shaded areas; mm/day) and 850-hPa winds (vectors; m/s) between 28th–29th pentad mean and 25th–26th pentad mean for CFSv2 predictions in (**a**) LD1; (**b**) LD5; (**c**) LD10; (**d**) LD15; (**e**) LD20; (**f**) LD25; (**g**) LD30; and (**h**) LD35.

From the above analysis, the skills of CFSv2 in predicting the changes in MC rainfall during the WTD and the DTW depend on the model's skills in predicting the large-scale rainfall changes. To provide a quantitative assessment of the model's prediction skills, we carry out a pattern correlation analysis (correlation between model results of different leads and observation) for the difference in rainfall over the area of 30°S–30°N/60°E–160°E. (It should be pointed out that the results obtained are not sensitive to the size of the area analyzed.) Following previous studies [50,51], we use the correlation coefficient of 0.5 as a threshold for skillful prediction. As seen from Figure 13, the prediction skill of CFSv2 for the WTD is higher than that for the DTW in all leads. The prediction skill of the model for the WTD gradually decreases from LD0 to LD15 and the correlation coefficient is lower than 0.5 when the lead time is longer than 23 days (about three weeks). For the DTW, the prediction skill of the model decreases rapidly from LD0 to LD5, and the correlation coefficient is lower than 0.5 when the lead time is longer than 15 days (about two weeks).

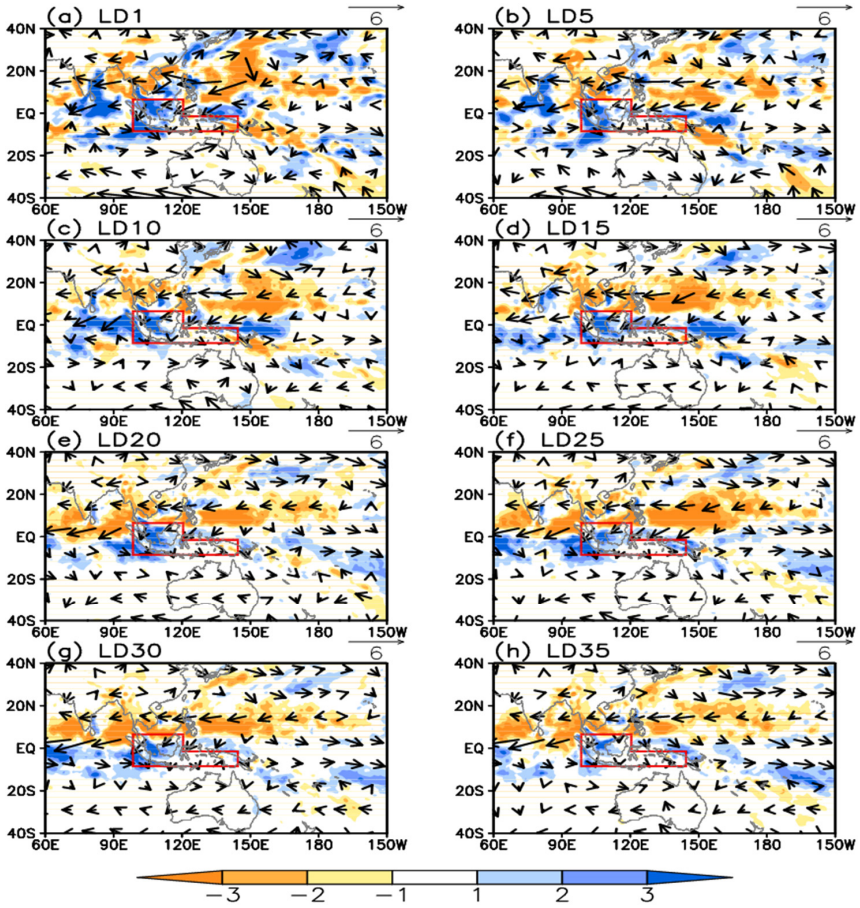

Figure 12. Differences in rainfall (shaded areas; mm/day) and 850-hPa winds (vectors; m/s) between 60th–61st pentad mean and 57th–58th pentad mean for CFSv2 predictions in (**a**) LD1; (**b**) LD5; (**c**) LD10; (**d**) LD15; (**e**) LD20; (**f**) LD25; (**g**) LD30; and (**h**) LD35.

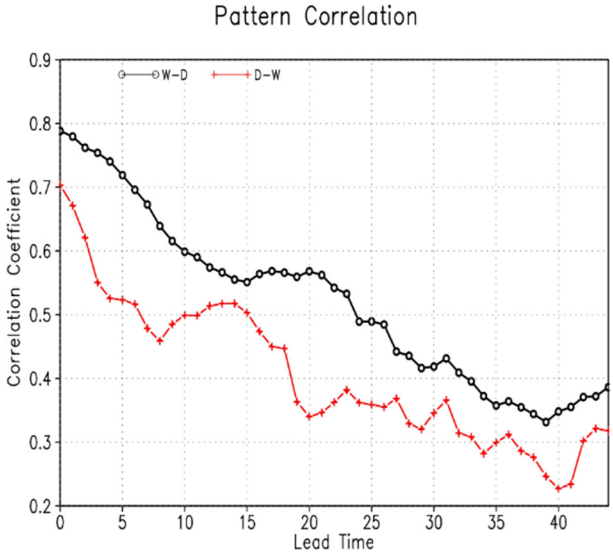

Figure 13. Coefficients of correlation between the differences in rainfall over 30°S–30°N/60°E–160°E for observation (GPCP) and for CFSv2. The black line denotes the correlation coefficients for differences between 28th–29th pentad mean and 25th–26th pentad mean, and the red line denotes the correlation coefficients for differences between 60th–61st pentad mean and 57th–58th pentad mean.

5. Discussion and Conclusions

Rainfall over the MC is dominated by a distinct annual cycle and its seasonal evolution is characterized by a wet season and a dry season. Previous studies have mainly focused on the seasonal-interannual and diurnal variations and their predictions of the MC rainfall [1–5], while characteristics and predictions of the MC rainfall for the transitional periods between the wet and dry seasons have received less attention. In this study, we have analyzed the features of the MC rainfall and the associated atmospheric circulation of the wet-dry transitional seasons and the skills of predicting these transitional features by the NCEP CFSv2.

Over the MC, the WTD occurs around the 27th pentad and the DTW occurs around the 59th pentad. This result is reliable given the consistency between the analyses of both CMAP and GPCP data sets. The MC rainfall experiences a sudden decrease during the WTD, contributing to a spatial coherency of timing for the WTD over the MC. On the other hand, a gradual increase in rainfall from the northern MC to the southern MC and from the western MC to the eastern MC takes place during the DTW, contributing to a later DTW for the southeastern MC than that for the western MC. The rainfall decrease during the WTD is accompanied by enhancement of the southeasterly monsoon winds, and the weakening of the easterlies over the equatorial Indian Ocean and the westerlies over the equatorial Pacific Ocean. The Australia High weakens as well. On the other hand, the WPSH intensifies and extends northeastward. These changes in circulation cause an anomalous lower-level divergence and upper-level convergence over the MC during the WTD, which is responsible for the decrease in rainfall over the MC. For the DTW, the Mascarene High weakened and an anomalous anticyclonic circulation appeared to the northeast of the Philippines at the lower troposphere. An anomalous low-level wind convergence occurs over the western MC during the DTW. Nevertheless, our analysis shows an asymmetric feature for the seasonal transition, but a full understanding of the reasons for this asymmetry requires further investigations.

The NCEP CFSv2 is able to capture the major features of the rainfall and related atmospheric circulation during the WTD and the DTW in LD0. However, the model underestimates the amplitude of rainfall changes for both the WTD and the DTW. This underestimation is contributed by the less-than-observed rainfall to the south of 2.5°N from the 17th pentad to the 26th pentad and to the north of the equator from the 54th pentad to the 60th pentad. Also, the WPSH and its changes during the two transitions are weaker than those in the observations, consistent with the result of Jiang *et al.* [41].

The CFSv2 predicts the major features of rainfall and the related atmospheric circulation well when the forecast lead time is less than three weeks for WTD and two weeks for DTW. The amplitudes of rainfall changes for both the WTD and DTW become smaller as the lead time increases. When the lead time is longer than 25 days, the changes in the winds over the western Pacific Ocean are almost opposite with those observed (westerly winds in the observation but easterly winds in the model) during the WTD. In the mean time, the changes in the winds over the equatorial Indian Ocean are well captured by the model for all leads. For the DTW, the model predicts much smaller amplitudes for the changes in rainfall over the MC and the associated atmospheric circulation patterns.

In this study, we have mainly focused on the climatological features of MC rainfall as well as the associated atmospheric circulation for both the WTD and DTW. The time of the WTD is the 27th, 26th, 27th, 27th, 33rd, 21st, 37th, 28th, 27th, and 32nd pentad for 2000–2009 (rainfall did not exhibit apparent dry and wet seasons in 2010), respectively (figure not shown). The time of the DTW is the 64th, 59th, 62nd, 56th, 65th, 58th, 69th, 59th, 59th, and 63rd pentad for 2000–2009, respectively (figure not shown). As examples, the time series of the pentad mean MC rainfall in the observation and CFSv2 of different leads for 2006 and 2008 are examined (Figures 14 and 15). The time of the WTD and that of the DTW in 2006 are later than those of other years, and the amplitude of rainfall decrease (increase) during the WTD (DTW) in 2006 is larger than that of climatology (black line in Figure 14). The MC rainfall variations during the WTD and the DTW in 2006 are well predicted by the CFSv2 within 10 lead days (Figure 14). The time of WTD (DTW) in 2006 is predicted by one pentad (two to four pentads) later

than in observations when the lead time is longer than 15 days (Figure 14). For 2008, the time of the WTD and the DTW is exactly the same as that in climatology (black line in Figure 15). The model predicts the MC rainfall variation during the WTD well within five lead days, and then the MC rainfall variation during the WTD is unrealistically predicted (Figure 15). On the other hand, the MC rainfall variation during the DTW is well represented by the CFSv2 within 30 lead days, which is much better than the prediction for the WTD (Figure 15). These WTD and DTW phases as well as their predictions vary from year to year, and the interannual variability of these transitional features needs to be further studied. It should be pointed out that the variations of rainfall over the northeastern MC have not been studied in the current analysis. Moreover, the prediction of these transitional features has not been fully addressed previously. Therefore, further studies are needed for enhancing our understanding of the MC rainfall variability and its prediction in different temporal and spatial scales.

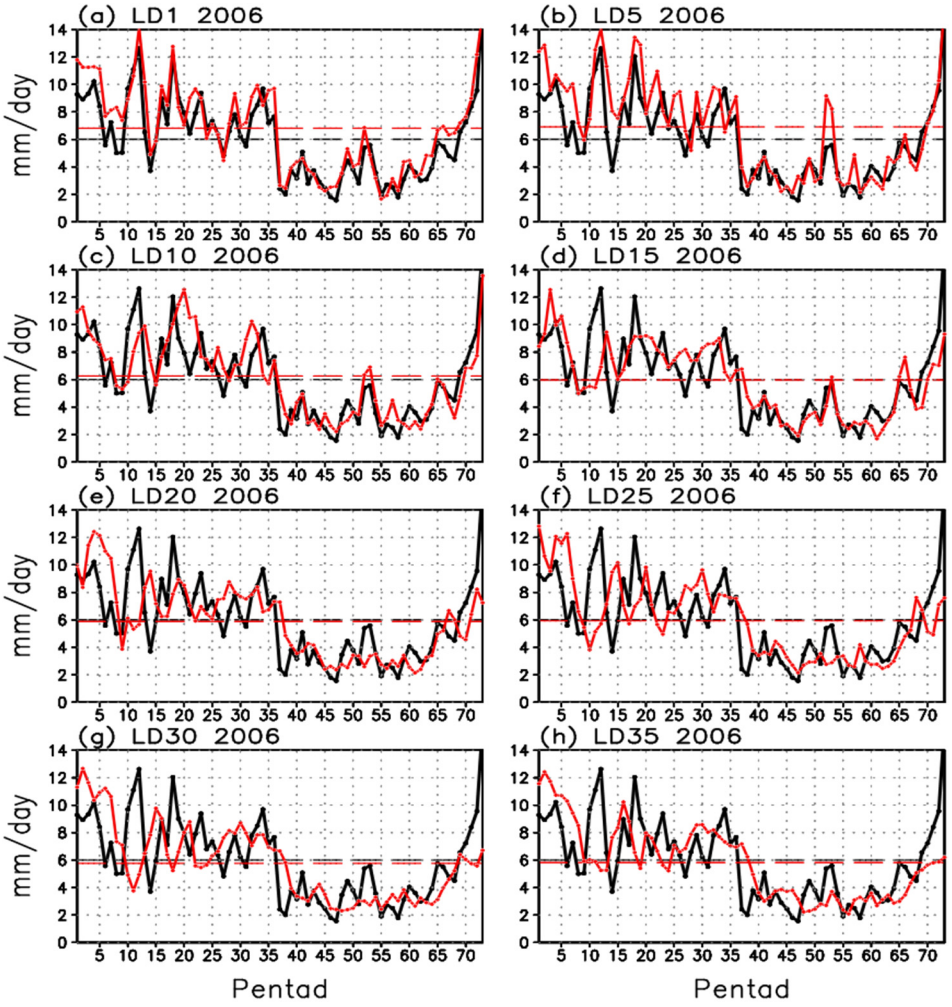

Figure 14. Pentad mean rainfall (mm/day) averaged over the Maritime Continent in 2006 for observation (GPCP; black line) and CFSv2 predictions (red line) in (**a**) LD1; (**b**) LD5; (**c**) LD10; (**d**) LD15; (**e**) LD20; (**f**) LD25; (**g**) LD30; and (**h**) LD35.

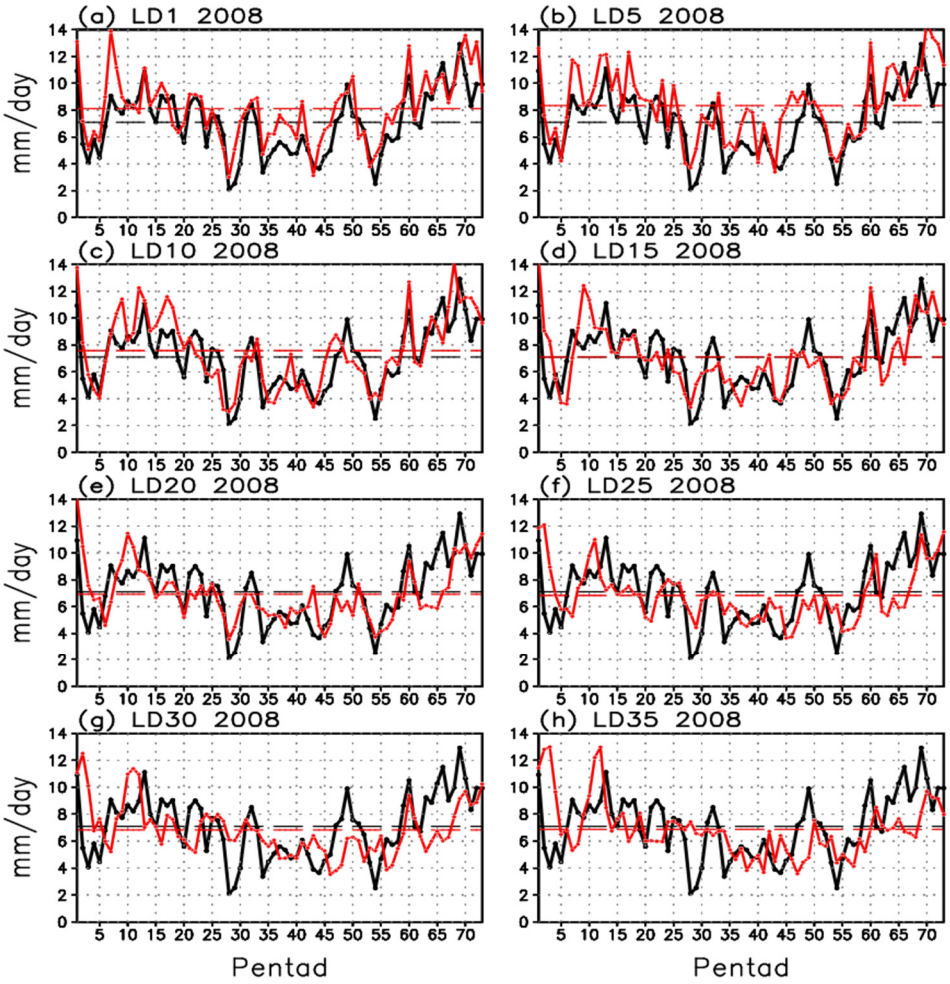

Figure 15. Same as in Figure 14, but for 2008. (**a**) LD1; (**b**) LD5; (**c**) LD10; (**d**) LD15; (**e**) LD20; (**f**) LD25; (**g**) LD30; and (**h**) LD35.

Acknowledgments: We thank the three anonymous reviewers and the editor for the constructive comments on the earlier version of the manuscript. This study was jointly supported by the National Basic Research Program of China (Grants 2014CB953900 and 2012CB956002), the National Natural Science Foundation of China (Grants 41375081 and 91337107), the LASW State Key Laboratory Special Fund (2013LASW-A05), the Jiangsu Collaborative Innovation Center for Climate Change, and the Zhuhai Joint Innovative Center for Climate, Environment and Ecosystem.

Author Contributions: Song Yang and Xingwen Jiang conceived and identified the framework of this study. Tuantuan Zhang analyzed data, carried out computation, prepared the manuscript. Shaorou Dong provided suggestions and technical support. All authors discussed the results and made contributions to the revision of the manuscript.

Conflicts of Interest: The authors declare no conflict of interest.

References

1. Chang, C.-P.; Wang, Z.; McBride, J.; Liu, C. Annual cycle of southeast Asia-Maritime Continent rainfall and the asymmetric monsoon transition. *J. Clim.* **2005**, *18*, 287–301. [CrossRef]
2. Lau, K.-M.; Chang, C.-P.; Chan, P.H. Short-term planetary-scale interactions over the tropics and midlatitudes. Part II: Winter MONEX period. *Mon. Weather Rev.* **1983**, *111*, 1372–1388. [CrossRef]
3. Meehl, G.A. The annual cycle and interannual variability in the tropical Pacific and Indian Ocean regions. *Mon. Weather Rev.* **1987**, *115*, 27–50. [CrossRef]
4. Matsumoto, J. The seasonal changes in Asian and Australian monsoon regions. *J. Meteorol. Soc. Jpn.* **1992**, *70*, 257–273.

5. Matsumoto, J.; Murakami, T. Seasonal migration of monsoons between the Northern and Southern Hemispheres as revealed from equatorially symmetric and asymmetric OLR data. *J. Meteorol. Soc. Jpn.* **2002**, *80*, 419–437. [CrossRef]
6. Yasunari, T. The monsoon year—A new concept of the climatic year in the Tropics. *Bull. Am. Meteorol. Soc.* **1991**, *72*, 1331–1338. [CrossRef]
7. Ramage, C.S. Role of a tropical "Maritime Continent" in the atmospheric circulation. *Mon. Weather Rev.* **1968**, *96*, 365–369. [CrossRef]
8. Qian, J.H. Why rainfall is mostly concentrated over islands in the Maritime Continent. *J. Atmos. Sci.* **2008**, *65*, 1428–1441. [CrossRef]
9. Simpson, J.; Keenan, T.D.; Ferrier, B.; Simpson, R.H.; Holland, G.J. Cumulus merger in the Maritime Continent region. *Meteorol. Atmos. Phys.* **1993**, *51*, 73–99. [CrossRef]
10. Hastenrath, S.; Lamb, P.J. Climate dynamics of atmosphere and ocean in the equatorial zone: A synthesis. *Int. J. Climatol.* **2004**, *24*, 1601–1612. [CrossRef]
11. Agudelo, P.A.; Curry, J.A.; Hoyos, C.D.; Webster, P.J. Transition between suppressed and active phases of intraseasonal oscillations in the Indo-Pacific warm pool. *J. Clim.* **2006**, *19*, 5519–5530. [CrossRef]
12. McBride, J.L.; Nicholls, N. Seasonal relationships between Australian rainfall and the Southern Oscillation. *Mon. Weather Rev.* **1983**, *111*, 1998–2004. [CrossRef]
13. McBride, J.L.; Haylock, M.R.; Nicholls, N. Relationships between the Maritime Continent heat source and the El Niño-Southern Oscillation phenomenon, *J. Clim.* **2003**, *16*, 2905–2914. [CrossRef]
14. Yang, G.-Y.; Slingo, J. The diurnal cycle in the tropics. *Mon. Weather Rev.* **2001**, *129*, 784–801. [CrossRef]
15. Keenan, T.D.; Rutledge, S.A.; Carbone, R.E.; Wilson, J.W.; Takahashi, T.; May, P.; Tapper, N.; Platt, M.; Hacker, J.M.; Sekelsky, S.M.; *et al*. The Maritime Continent Thunderstorm Experiment (MCTEX): Overview and some results. *Bull. Am. Meteorol. Soc.* **2000**, *81*, 2433–2455. [CrossRef]
16. Keenan, T.D.; Morton, B.R.; Manton, M.J.; Holland, G.J. The Island Thunderstorm Experiment (ITEX): A study of tropical thunderstorms in the Maritime Continent. *Bull. Am. Meteorol. Soc.* **1989**, *70*, 152–159. [CrossRef]
17. Inness, P.M.; Slingo, J.M. The interaction of the MJO with the Maritime Continent in a GCM. *Q. J. R. Meteorol. Soc.* **2006**, *132*, 1645–1667. [CrossRef]
18. Chang, C.-P.; Lau, K.-M. Short-term planetary-scale interactions over the tropics and midlatitudes during northern winter. Part I: Contrasts between active and inactive periods. *Mon. Weather Rev.* **1982**, *110*, 933–946. [CrossRef]
19. Chang, C.-P.; Harr, P.A.; Chen, H.-J. Synoptic disturbances over the equatorial South China Sea and western Maritime Continent during boreal winter. *Mon. Weather Rev.* **2005**, *133*, 489–503. [CrossRef]
20. Slingo, J.M.; Inness, P.M.; Neale, R.B.; Woolnough, S.J.; Yang, G.Y. Scale interactions on diurnal to seasonal timescales and their relevance to model systematic errors. *Ann. Geophys.* **2003**, *46*, 139–155.
21. Sui, C.H.; Lau, K.M. Multiscale phenomena in the tropical atmosphere over the Western Pacific. *Mon. Weather Rev.* **1992**, *120*, 407–430. [CrossRef]
22. Zhu, B.; Wang, B. The 30–60-day convection seesaw between the tropical Indian and western Pacific oceans. *J. Atmos. Sci.* **1993**, *50*, 184–199. [CrossRef]
23. Zhang, Y.; Sperber, K.S.; Boyle, J.S. Climatology and interannual variation of the East Asia winter monsoon: Results from the 1979–95 NCEP/NCAR Reanalysis. *Mon. Weather Rev.* **1997**, *125*, 2605–2619. [CrossRef]
24. Park, T.-W.; Ho, C.-H.; Yang, S. Relationship between the Arctic Oscillation and cold surges over East Asia. *J. Clim.* **2011**, *24*, 68–83. [CrossRef]
25. Holland, G.J.; Keenan, T.D. Diurnal variations of convection over the "Maritime Continent". *Mon. Weather Rev.* **1980**, *108*, 223–225. [CrossRef]
26. McBride, J.L. *Tropical Cyclone Formation. Global Perspective on Tropical Cyclones*; Elsberry, R.L., Ed.; Tech. Doc. 693; World Meteorological Organization: Geneva, Switzerland, 1995; pp. 63–105.
27. Inness, P.M.; Slingo, J.M.; Guilyardi, E.; Cole, J. Simulation of Madden-Julian Oscillation in a coupled general circulation model. Part II: The role of the basic state. *J. Clim.* **2003**, *16*, 365–382. [CrossRef]
28. Hendon, H.H. Indonesian rainfall variability: Impacts of ENSO and local air-sea interaction. *J. Clim.* **2003**, *16*, 1775–1790. [CrossRef]
29. Haylock, M.; McBride, J. Spatial coherence and predictability of Indonesian wet season rainfall. *J. Clim.* **2001**, *14*, 3882–3887. [CrossRef]

30. Horel, J.D.; Wallace, J.M. Planetary scale atmospheric phenomena associated with the Southern Oscillation. *Mon. Weather Rev.* **1981**, *109*, 813–829. [CrossRef]
31. Zhang, T.; Yang, S.; Jiang, X.; Zhao, P. Seasonal-interannual variation and prediction of wet and dry season rainfall over the Maritime Continent: Roles of ENSO and monsoon circulation. *J. Clim.* **2015**. [CrossRef]
32. Aldrian, E.; Gates, L.D.; Widodo, F.H. Seasonal variability of Indonesia rainfall in ECHAM4 simulations and in the reanalyses: The role of ENSO. *Theor. Appl. Climatol.* **2007**, *87*, 41–59. [CrossRef]
33. Hung, C.-W.; Yanai, M. Factors contributing to the onset of the Australian summer monsoon. *Q. J. R. Meteorol. Soc.* **2004**, *130*, 739–761. [CrossRef]
34. Hung, C.-W.; Liu, X.; Yanai, M. Symmetry and asymmetry of the Asian and Australian summer monsoons. *J. Clim.* **2004**, *17*, 2413–2426. [CrossRef]
35. Li, T.; Philander, S.G.H. On the annual cycle of the eastern equatorial Pacific. *J. Clim.* **1996**, *9*, 2986–2998. [CrossRef]
36. Wang, B. On the annual cycle in the tropical eastern and central Pacific. *J. Clim.* **1994**, *7*, 1926–1942. [CrossRef]
37. Webster, P.J.; Palmer, T.; Yanai, M.; Tomas, R.; Magana, V.; Shukla, J.; Yasunari, T. Monsoons: Processes, predictability and the prospects for prediction. *J. Geophys. Res.* **1998**, *103*, 14451–14510. [CrossRef]
38. Matsumoto, J.; Murakami, T. Annual changes of tropical convective activities as revealed from equatorial symmetric OLR data. *J. Meteorol. Soc. Jpn.* **2000**, *78*, 543–561.
39. Jiang, X.; Li, J. Influence of the annual cycle of SST on the monsoon onset. *J. Geophys. Res.* **2011**, *116*, D10105. [CrossRef]
40. Neale, R.; Slingo, J. The Maritime Continent and its role in the global climate: A GCM study. *J. Clim.* **2003**, *16*, 834–848. [CrossRef]
41. Jiang, X.; Yang, S.; Li, Y.; Kumar, A.; Wang, W.; Gao, Z. Dynamical prediction of the East Asian winter monsoon by the NCEP Climate Forecast System. *J. Geophys. Res.* **2013**, *118*, 1312–1328. [CrossRef]
42. Jiang, X.; Li, Y.; Yang, S.; Shu, J.; He, G. Interannual variation of mid-summer heavy rainfall in the eastern edge of the Tibetan Plateau. *Clim. Dyn.* **2015**. [CrossRef]
43. Hackert, E.C.; Hastenrath, S. Mechanisms of Java rainfall anomalies. *Mon. Weather Rev.* **1986**, *114*, 745–757. [CrossRef]
44. Nicholls, N. A simple air-sea interaction model. *Q. J. R. Meteorol. Soc.* **1979**, *105*, 93–105. [CrossRef]
45. Wild, M.; Roeckner, E. Radiative fluxes in the ECHAM5 General Circulation Model. *J. Clim.* **2006**, *19*, 3792–3809. [CrossRef]
46. Mori, S.; Hamada, J.I.; Tauhid, Y.I.; Yamanaka, M.D.; Okamato, N.; Murata, F.; Sakurai, N.; Hashiguchi, H.; Sribimawati, T. Diurnal land-sea rainfall peak migration over Sumatera Island, Indonesian Maritime Continent, observed by TRMM satellite and intensive rawinsonde soundings. *Mon. Weather Rev.* **2004**, *132*, 2021–2039. [CrossRef]
47. Ichikawa, H.; Yasunari, T. Time-space characteristics of diurnal rainfall over Borneo and surrounding oceans as observed by TRMMPR. *J. Clim.* **2006**, *19*, 1238–1260. [CrossRef]
48. Rauniyar, S.P.; Walsh, K.J.E. Influence of ENSO on the diurnal cycle of rainfall over the Maritime Continent and Australia. *J. Clim.* **2012**, *26*, 1304–1321. [CrossRef]
49. Madden, R.A.; Julian, P.R. Detection of a 40–50 day oscillation in the zonal wind in the tropical Pacific. *J. Atmos. Sci.* **1971**, *28*, 702–708. [CrossRef]
50. Kim, H.-M.; Webster, P.J.; Toma, V.E.; Kim, D. Predictability and prediction skill of the MJO in two operational forecasting systems. *J. Clim.* **2014**, *27*, 5364–5378. [CrossRef]
51. Wang, W.; Hung, M.-P.; Weaver, S.J.; Kumar, A.; Fu, X. MJO prediction in the NCEP Climate Forecast System version 2. *Clim. Dyn.* **2014**, *42*, 2509–2520. [CrossRef]
52. Zhang, Q.; Dool, H. Relative merit of model improvement *versus* availability of retrospective forecasts: The case of Climate Forecast System MJO prediction. *Weather Forecast.* **2012**, *27*, 1045–1051. [CrossRef]
53. Saha, S.; Moorthi, S.; Wu, X.; Wang, J.; Nadiga, S.; Tripp, P.; Behringer, D.; Hou, Y.T.; Chuang, H.Y.; Iredell, M.; Ek, M. The NCEP Climate Forecast System Version 2. *J. Clim.* **2013**, *27*, 2185–2208. [CrossRef]
54. Saha, S.; Nadiga, S.; Thiaw, C.; Wang, J.; Wang, W.; Zhang, Q.; van den Dool, H.M.; Pan, H.L.; Moorthi, S.; Behringer, D.; *et al*. The NCEP Climate Forecast System. *J. Clim.* **2006**, *19*, 3483–3517. [CrossRef]
55. Saha, S.; Moorthi, S.; Pan, H.L.; Wu, X.; Wang, J.; Nadiga, S.; Tripp, P.; Kistler, R.; Woollen, J.; Behringer, D.; *et al*. The NCEP Climate Forecast System Reanalysis. *Bull. Am. Meteorol. Soc.* **2010**, *91*, 1015–1057. [CrossRef]

56. Moorthi, S.; Pan, H.-L.; Caplan, P. *Changes to the 2001 NCEP Operational MRF/AVN Global Analysis/Forecast System*, 1st ed.; US Department of Commerce, National Oceanic and Atmospheric Administration, National Weather Service, Office of Meteorology, Program and Plans Division: Silver Spring, MD, USA, 2001; pp. 1–14.
57. Ek, M.B.; Mitchell, K.E.; Lin, Y.; Rogers, E.; Grunmann, P.; Koren, V.; Gayno, G.; Tarpley, J.D. Implementation of Noah land surface model advances in the national centers for environmental prediction operational mesoscale eta model. *J. Geophys. Res.* **2003**, 108–8851. [CrossRef]
58. Griffies, S.M.; Harrison, M.J.; Pacanowsky, R.C.; Rosati, A. *A Technical Guide to MOM4. GFDL Ocean Group Technical Report 5*; NOAA/GFDL: Princeton, NJ, USA, 2003; p. 295.
59. Kalnay, E.; Kanamitsu, M.; Kistler, R.; Collins, W.; Deaven, D.; Gandin, L.; Iredell, M.; Saha, S.; White, G.; Woollen, J.; *et al*. The NCEP/NCAR 40-year reanalysis project. *Bull. Am. Meteorol. Soc.* **1996**, *77*, 437–471. [CrossRef]
60. Adler, R.F.; Huffman, G.J.; Chang, A.; Ferraro, R.; Xie, P.P.; Janowiak, J.; Rudolf, B.; Schneider, U.; Curtis, S.; Bolvin, D.; *et al*. The version 2 Global Precipitation Climatology Project (GPCP) Monthly Precipitation Analysis (1979–present). *J. Hydrometeor.* **2003**, *4*, 1147–1167. [CrossRef]
61. Wang, B.; Ho, L. Rainy season of the Asian–Pacific summer monsoon. *J. Clim.* **2001**, *15*, 386–398. [CrossRef]